Eur. Phys. J. Appl. Phys. **93**, 10401 (2021)

https://doi.org/10.1051/epjap/2020200233

THE EUROPEAN PHYSICAL JOURNAL APPLIED PHYSICS

Regular Article

Impact of conduction band non-parabolicity and dielectric mismatch on photoionization cross section of donor bound polaron in spherical GaN/InN core-shell nanoparticle★

Abdelali Talbi[1,2,*], Mohamed El Haouari[2,3], Khalid Nouneh[1], El Mustapha Feddi[2], and Mohammed Addou[4]

[1] Laboratory of Materials Physics & Subatomics, Department of Physics, Faculty of Science, Ibn Tofail University, BP. 242, 14000, Kenitra, Morocco
[2] Group of Optoelectronic of Semiconductors and Nanomaterials, ENSAM de Rabat, Mohammed V University in Rabat, Rabat, Morocco
[3] Centre Régional des Métiers de l'Education et de Formation (CRMEF), Tanger 90060, Morocco
[4] Laboratory of Materials and Valorizations of Natural Resources, University Abdelmalek Essaadi, Tangier, Morocco

Received: 15 July 2020 / Received in final form: 10 October 2020 / Accepted: 17 November 2020

Abstract. Understanding the behavior of single dopant in semiconductors is a challenge to attain a high control on optoelectronic devices. Based on the fact that the external perturbations have an important impact on properties of doped nanocrystals, we have studied the simultaneous effects of phonons and conduction band non-parabolicity combined to dielectric mismatch and donor position on the photoionization cross section of an off-center donor in spherical *GaN/InN* core-shell quantum dots. The calculations were carried out within the framework of the effective-mass approximation and the eigenvalues equation has been solved using the Ritz variational method. The examination of the photoionization cross section, corresponding to the first donor energy level and the non-parabolic conduction band optical transition, shows clearly that the existence of non-parabolicity band or dielectric environment causes a blue shift of resonance peaks while the existence of phonon red shift them with a non-neglected variations in their intensity. The donor position has also an important effect on peaks position and amplitude.

1 Introduction

Semiconductor nanocrystals (SNs) are among the most studied materials that meet the needs of today's applications, such as biolabels sensors, light-emitting diode lasers and drugs. They are fluorescent nanoparticles whose radius is comparable to the Bohr exciton radius of the material.

In bulk, the materials dimensions are much bigger than the Bohr radius, thus the energies are continuous. Decreasing the size to be almost equal the Bohr exciton radius results a discretization of energy levels, this leads to a significant change in the electronic density of states (DOS) of charge carriers due to the spatial confinement of the wave function.

The Quantum dots (QD) are one of the most known nanoparticles groups. Once they are discovered by Alexei Ekimov in 1980s [1], the era of nanotechnology was begun. There has been much advancement in nanomaterials synthesis and nanotechnology research that demonstrated the QDs impact in different fields such science, engineering and healthcare.

Core-shell semiconductor nanoparticles have been broadly investigated in the last two decades. Reviews on the production of core-shell quantum dots (CSQDs) as well as their physical properties have recently appeared [2,3]. In many cases, fabricating CSQDs makes use of rather cheap chemical procedures which have made them most appealing to applications in the areas of photocatalysis and optoelectronics [4–6].

Generally speaking, there are three types of CSQDs; type-I, inverted type-I and type-II. They are classified based on the band alignment of their core/shell materials. Type-I (inverted type-I) has a shell (core) band gap bigger than that of the core (shell) which is confining electrons/holes in nanostructure core [7,8] (shell [9,10]). In type-II, valence and conduction bands of the core are both higher or lower than those of the shell taking the form of a cascade and leading to a spatial separation of opposite sign charge carriers i.e. electrons are in core while holes are in shell or vice versa [11,12].

Every type of the three has its advantages. Type-I is known by its high photoluminescence quantum yields [13–15] resulting from its high shell band gap which

★ Contribution to the Topical Issue "Advanced Materials for Energy Harvesting, Storage, Sensing and Environmental Engineering (ICOME 2019)", edited by Mohammed El Ganaoui, Mohamed El Jouad, Rachid Bennacer, Jean-Michel Nunzi.

* e-mail: abdelali.talbi@uit.ac.ma

passivats layer and suppresses the non-radiational recombination [16]. It also acts as a barrier that improves stability and precludes the polarization of electron-hole pairs.

Inverted type-I is known by its much more tunable emissions compared to type-I allowing benefiting from full color display [17]. Tuning the shell thickness provides a high control of emission wavelength. In such structure, the emission comes from the radiative recombinations of electrons and holes confined in the shell. In QD-based solar cells, this type favors the photogenerated electrons extraction and increases the electron injection rate benefiting of non-overcoming the shell big physical barrier as type-I case [9].

In type-II structure, the fact that electrons and holes are localized in two different regions decreases significantly the charge carriers recombination rate leading to a prolonged luminescence lifetime. Further, type-II structure can be emitter at wavelengths that cannot be carried out with any other two materials alone [18].

Regarding III-nitride-based QD structures we can find some interesting studies. Ghazi et al. [19] have investigated the magnetic field effect on donor states in *GaN/InGaN* CSQD. The properties of exciton in *GaN/InGaN* quantum dot-quantum well system have been investigated by Ganesan and Senthilkumar [20]. The nonlinear optical properties were also the subject of some papers, Elkadadra et al. have studied them in cubic structure [21] whereas Liu et al. in spherical one [22]. The choice of the III-V GaN/InN is encouraged by crystal tetrahedral structure of the both GaN and InN materials and also by the large difference between their gaps which make them suitable for reversed type-I CSQD. This choice is supported by their promising potential optoelectronic applications [23,24].

Adding impurities into nanostructures is an efficient way to control their properties [25]. It's well known that during the growth process it may be unintentionally having impurities due to the non-purity of the precursors or to the non-total cleanliness of used equipment. Recently, experimental developments allow to having, manipulating and even controlled positioning single dopants into nanostructures [26,27]. The presence of single dopant influences considerably optical, electric and magnetic semiconductors properties which opens the door to improve many optoelectronic devices. Moreover, the impurities-excitons binding can provide a better understanding to photoluminescence transitions [28–31].

On the other side, ionic and weakly ionic materials as the nitride-based nanocrystals have an electron-polar interactions that cannot be neglected, they are coming from the renormalized electron-phonon effective mass and the edge energy of conduction band [32–34]. The influence of polaronic corrections on impurity states in QD has been investigated in some papers [35,36]. Another work can be mentioned, is that of Sali et al. in which they have studied the phonon and conduction non-parabolicity band (NPB) effects on the binding energy of on-center impurity in a spherical GaAs QD [37]. In a recent paper, we have reported a theoretical study on impurity bound polaron influence in GaN/InN CSQDs taking into consideration the band non-parabolicity effects [38].

The CSQDs are frequently surrounded by a dielectric medium. Thus, the dielectric mismatch (DMM) between the core and shell layers or between the shell and the surrounding medium creates image charges that modify electron-donor electrostatic potential. Several authors have studied the effect of DMM on cubic, spherical and cylindrical forms [39–42]. Cristea and Niculescu have investigated the CSQDs geometry [43–46]. Vartanian and his team have reported a work concerning dielectric mismatch and polaron effects on impurity optical response of spherical QDs [47].

In a recent work, we have investigated phonons and donor position effects on the binding energy and on the photoionization cross section (PCS) for CdTe and ZnSe materials. The calculations were done in the framework of a simple infinite confining potential system. The resonance peaks of PCS have been red shifted when the effect of electron-LO-phonon interactions are taken into consideration or when the donor is moved away from the center to the shell edges [48]. In this paper, in addition to electron-LO-phonon corrections and donor position, we have investigated the effect of the conduction non parabolic band and the dielectric mismatch on the PCS of single impurity confined in zinc blende (ZB) GaN/InN CSQD. This time, the confining potential is chosen to be more realistic as a finite barrier. The theoretical approach, methods and calculation conditions are presented in Section 2. Numerical results and discussions are given in Section 3. Conclusions are outlined in Section 4.

2 Theoretical framework

We consider a *GaN/InN* spherical *CSQD* composed of a core with radius a wrapped by a shell with radius b. The hydrogenic impurity D^0 is assumed to be in the shell region along to the z-axis (see Fig. 1). We emphasize that the whole structure is embedded in a dielectric medium characterized by a large band gap and a small dielectric constant such as SiO_2 ($\varepsilon = 3.9$) and $BaTiO_3$-ferroelectric ($\varepsilon = 5$). To take into consideration the image charge effects caused by the surrounding dielectric matrix we have fixed the dielectric constant of the structure as $\varepsilon_{in} = \sqrt{\varepsilon_c \varepsilon_s}$, where $\varepsilon_c = \varepsilon_{GaN}$ and $\varepsilon_s = \varepsilon_{InN}$, and that of the external medium as ε_{out} [43,49].

Besides, the electron-LO-phonon interaction has been treated applying the bulk-like description of the polaronic effect via the well-known Fröhlich model and adopted subsequently to the Bajaj and Aldrich model in order to provide a better description to the Coulombic coupling [50–52]. Here, we may recall that LA, TA and TO phonons have not been taking into consideration since the Frohlich approach judge them null and can be neglected. For more details see references [52,53].

Furthermore, we suppose that, around the Γ-point, the material conduction band is influenced by the

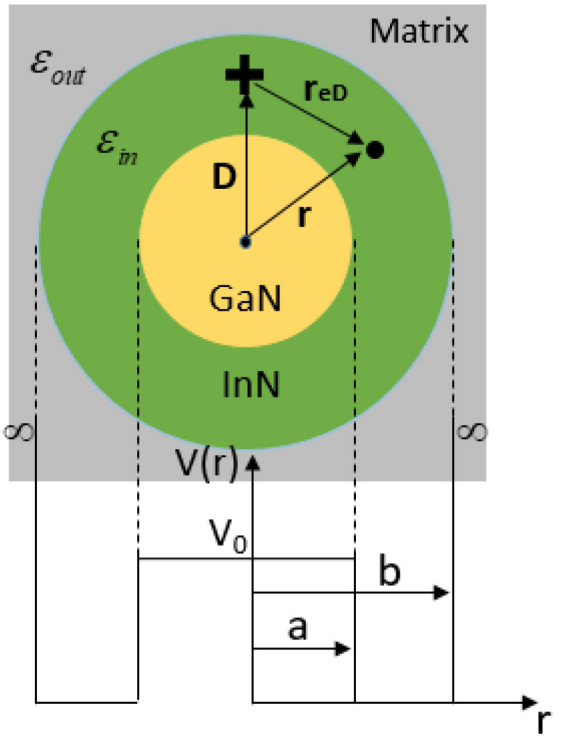

Fig. 1. Schematic representation of core/shell Quantum Dot structure.

non-parabolicity phenomenon which leads to an energy-dependent polaron effective mass written as follow [54–56].

$$\mathrm{m}_e^*(\mathrm{i},\mathrm{E}) = \mathrm{m}_{e,i}^*\left(1+\frac{E-\mathrm{V}_i}{E_{i,g}}\right) \tag{1}$$

where 'i' labels each material and V_i is the confinement potential given, as a function of the radial position, by [57].

$$V_w(r) = \begin{cases} Q\Delta E_g, & 0 \le r \le a \\ 0, & a < r \le b \\ \infty, & r > b \end{cases} \tag{2}$$

where $Q = 0.7$ is the conduction band offset parameter defined as 70|30 between conduction and valence bands [57,58]. ΔE_g is the difference between the core (GaN) and the shell (InN) band gaps at Γ-point:

$$\Delta\mathrm{E}_g = \left[\mathrm{E_g(GaN)} - \mathrm{E_g(InN)}\right]. \tag{3}$$

The existence of external dielectric medium around the structure requires additional terms in the potential energy. Firstly, we have the Coulombic energy [45,46].

$$V_c = -\frac{e^2}{\varepsilon_{\mathrm{in}} r_{\mathrm{eD}}} - \frac{e^2(\varepsilon_{\mathrm{in}}-\varepsilon_{\mathrm{out}})}{\varepsilon_{\mathrm{in}} b} \times \sum_{k=0}^{\infty} \frac{k+1}{k\varepsilon_{\mathrm{in}} + (1+k)\varepsilon_{\mathrm{out}}} \left(\frac{D r_{\mathrm{eD}}}{b^2}\right)^k P_k(\cos(\theta)) \tag{4}$$

which represents the electron-impurity electrostatic interaction including both, the Coulomb potential and the image charge of the impurity; this last depends on the donor position. For off-centre donor, it is given as above. Where, $r_{\mathrm{eD}} = \sqrt{r^2 + D^2 - 2rD\cos(\theta)}$ is the donor-electron distance, and θ is the angle between their vectors position r and D. $P_k(\cos(\theta))$ is the k^{th}-order of Legendre polynomial.

As well, there is another term that represents the electron self-energy originate from the interaction with its image-charge [59].

$$W(r) = \frac{e^2(\varepsilon_{\mathrm{in}} - \varepsilon_{\mathrm{out}})}{2\varepsilon_{\mathrm{in}} b} \sum_{k=0}^{\infty} \frac{k+1}{k\varepsilon_{\mathrm{in}} + (1+k)\varepsilon_{\mathrm{out}}} \left(\frac{r}{b}\right)^{2k}. \tag{5}$$

On the other side, the non-interacting LO-phonon Hamiltonian in the two regions ($i = c,\ s$) has the form [35]:

$$H_{ph} = \sum_{lmq} \hbar\omega_{LO_i} \left(a_{lm}^{\dagger}(q) a_{lm}(q) + \frac{1}{2}\right) \tag{6}$$

$a_{lm}^{\dagger}(q)$ and $a_{lm}(q)$ are, respectively, the creation and the annihilation operators, l and m are the azimuthal and magnetic quantum numbers and ω_{LO_i} is the LO-phonon frequency. The electron-LO phonon coupling Hamiltonian in Fröhlich framework will be [52]:

$$H_{i,e-ph} = \sum \left(V_{q,i} e^{iqr} a_q + V_{q,i}^* e^{-iqr} a_q^{\dagger}\right) \tag{7}$$

$V_{q,i}$ is the amplitude interaction given by:

$$V_{q,i} = -\frac{i\hbar\omega_{LO_i}}{q} \left(\frac{4\pi\alpha_i}{\Omega}\right)^{1/2} \left[\frac{\hbar}{2m_e^*(i,E)\omega_{LO_i}}\right]^{1/4} \tag{8}$$

where Ω is the volume of the structure and α is the coefficient of the electron-LO-phonon dimensionless coupling coefficient, it's given as: $\alpha_i = \left(\frac{e^2\eta_i}{2\varepsilon_i'\hbar\omega_{LO_i}}\right)$.

Whereas $\eta_i = \left(\frac{2m_e^*(i,E)\omega_{LO_i}}{\hbar}\right)^{1/2}$ and $\frac{1}{\varepsilon_i'} = \frac{1}{\varepsilon_{\infty,i}'} - \frac{1}{\varepsilon_{0,i}}$.

Further, the energy-dependent effective mass of polaron, in each material, has the form [40]:

$$m_{ep}^*(i,E) = m_e^*(i,E)\frac{1+\alpha_i/12}{1-\alpha_i/12}. \tag{9}$$

Based on the above information, the effective Hamiltonian of Aldrich-Bajaj can be expressed as [40,60,61]:

$$H_{i,\mathrm{eff}} = -\frac{\hbar^2}{2}\overline{\nabla}\frac{1}{m_{ep}(i,E)}\overline{\nabla} + V_w + V_{\mathrm{eff}}^i \tag{10}$$

V_{eff} is the renormalized phonon energy comprising the Coulombic potential [40].

$$V_{\text{eff}}^{i} = -\frac{e^2}{\varepsilon_{0,i} r_{\text{eD}}} - \frac{e^2}{\varepsilon_i' r_{\text{eD}}} \exp(-\eta_i r_{\text{eD}}) + \frac{e\eta_i}{2\varepsilon_i'} \frac{\exp(-\eta_i r_{\text{eD}})}{1 + \alpha_i/12 + \alpha_i/(4 + \alpha_i/3)} - \alpha_i \hbar \omega_{LO_i}. \tag{11}$$

Here, it's worth mentioning that due to ZB structure symmetry the built-in electric field term (BEF) comes from piezoelectricity and spontaneous has not been taken into account. So, pay attention that for wurtzite nitride structure, BEF shouldn't be neglected [23].

To simplify the writing of the equations, we use the effective Bohr radius $a_D = \frac{\hbar^2 \varepsilon_{\text{in}}}{m_{epc(E)} e^2} = 12.9\,\text{nm}$ as unit of length, and the effective Rydberg $R_D = \frac{e^2}{2\varepsilon_{\text{in}} a_D^2} = 5.42\,\text{meV}$ as unit of energy. Thus, the Hamiltonian for the core and the shell regions can be simplified, respectively, as follow:

See equation below.

where

$$V_{\text{eff}}^{1} = -\frac{\varepsilon_{\text{in}}}{\varepsilon_c' r_{\text{eD}}} \exp(-\eta_c r_{\text{eD}}) + \frac{\varepsilon_{\text{in}}}{\varepsilon_c'} \eta_c \frac{\exp(-\eta_c r_{\text{eD}})}{1 + \alpha_c/12 + \alpha_c/(4 + \alpha_c/3)} - \alpha_c \hbar \omega_{LO_c}/R_D$$

$$V_{\text{eff}}^{2} = -\frac{\varepsilon_{\text{in}}}{\varepsilon_s' r_{\text{eD}}} \exp(-\eta_s r_{\text{eD}}) + \frac{\varepsilon_{\text{in}}}{\varepsilon_s'} \eta_s \frac{\exp(-\eta_s r_{\text{eD}})}{1 + \alpha_s/12 + \alpha_s/(4 + \alpha_s/3)} - \alpha_s \hbar \omega_{LO_s}/R_D.$$

Without the impurity, the wave function of electron writes: $\psi(r, \theta, \varphi) = R_n(r)\, Y_{l,m}(\theta_e, \varphi_e)$. $R_n(r)$ is the radial part, $Y_{l,m}(\theta_e, \varphi_e)$ are the spherical harmonics, n, l and m are, respectively, the main, azimuthal and magnetic quantum numbers. Here, we consider only the ground state energy corresponding to $n = 1$, $l = 0$ and $m = 0$ configuration.

The confinement potential and the core/shell radii determine the electron position. There are two possibilities: either in the core for $E_e^{1s} < V_{0e}$ or in the shell for $E_e^{1s} \geq V_{0e}$. In the first case we have [38,62,63]:

$$\psi_e(r) = \frac{1}{r} \begin{cases} N_1 \sinh(k_1 r), & 0 \leq r \leq a \\ N_2 \sin[k_2(r-b)], & a < r \leq b \end{cases} \tag{12}$$

where $k_1 = \sqrt{(V_{0e} - E_e^{1s})/R_D}$, $k_2 = \sqrt{E_e^{1s}/\sigma(E) R_D}$ and $\sigma(E) = m_{ep}(c, E)/m_{ep}(s, E)$.

In the second case the wave function turns to [38,62,63]:

$$\psi_e(r) = \frac{1}{r} \begin{cases} N_3 \sin(k_3 r), & 0 \leq r \leq a \\ N_4 \sin[k_4(r-b)], & a < r \leq b \end{cases} \tag{13}$$

where $k_3 = \sqrt{(E_e^{1s} - V_{0e})/R_D}$ and $k_4 = \sqrt{E_e^{1s}/\sigma(E) R_D}$. In both cases N_i are the normalization constants that we can calculate via the condition $\langle \psi_e | \psi_e \rangle = 1$. The ground state energy E_e^{1s} is determined by solving the transcendental equation resulting from the continuity equations of the wave function and the probability current densities at the core surface:

$$[\psi_{\text{core}}(r)]_{r=a^-} = [\psi_{\text{shell}}(r)]_{r=a^+} \tag{14}$$

$$\left[\frac{1}{m_{ep}(c,E)} \frac{d\psi_{\text{core}}(r)}{dr}\right]_{r=a^-} = \left[\frac{1}{m_{ep}(s,E)} \frac{d\psi_{\text{shell}}(r)}{dr}\right]_{r=a^+} \tag{15}$$

where a^- and a^+ denote the core and the shell sides of the interface respectively.

The donor ground state energy E_{D^0} and the corresponding envelope wave function are solutions of the Schrödinger equation:

$$H\psi(r, \theta, \phi) = E_{D^0} \psi(r, \theta, \phi). \tag{16}$$

This eigenvalue equation, which has no analytical solution, can be solved using a variational approach. The trial wave function is as:

$$\psi_{D^0}(r, \theta, \phi) = N \psi_e(r) e^{-\beta r_{\text{eD}}}. \tag{17}$$

$$H_1 = -\Delta - \frac{2}{r_{\text{eD}}} - \frac{2(\varepsilon_{\text{in}} - \varepsilon_{\text{out}})}{b} \sum_{k=0}^{\infty} \frac{k+1}{k\varepsilon_{\text{in}} + (1+k)\varepsilon_{\text{out}}} \left(\frac{D r_{\text{eD}}}{b^2}\right)^k$$

$$P(\cos(\theta)) + \frac{2(\varepsilon_{\text{in}} - \varepsilon_{\text{out}})}{b} \sum_{k=0}^{\infty} \frac{k+1}{k\varepsilon_{\text{in}} + (1+k)\varepsilon_{\text{out}}} \left(\frac{r}{b}\right)^{2k} + V_0 + V_{\text{eff}}^{1}$$

$$H_2 = -\sigma(E)\Delta - \frac{2}{r_{\text{eD}}} - \frac{2(\varepsilon_{\text{in}} - \varepsilon_{\text{out}})}{b} \sum_{k=0}^{\infty} \frac{k+1}{k\varepsilon_{\text{in}} + (1+k)\varepsilon_{\text{out}}} \left(\frac{D r_{\text{eD}}}{b^2}\right)^k$$

$$P(\cos(\theta)) + \frac{2(\varepsilon_{\text{in}} - \varepsilon_{\text{out}})}{b} \sum_{k=0}^{\infty} \frac{k+1}{k\varepsilon_{\text{in}} + (1+k)\varepsilon_{\text{out}}} \left(\frac{r}{b}\right)^{2k} + V_{\text{eff}}^{2}$$

Table 1. Input parameters for zinc-blende *GaN* and *InN* at low temperature (see Refs. [74–77]).

Material	Parameters				
	m_e^*/m_0	ε_0	ε_∞	$E_g(eV)$	$\omega_{LO}(cm^{-1})$
GaN	0.193	9.44	5.31	3.3	742
InN	0.054	11.22	7.0	0.60	590

By minimizing the expectation value of H against the variational parameter β we can determine the impurity ground state energy.

$$E_{D^0} = \min_{\beta} \frac{\langle\psi|H|\psi\rangle}{\langle\psi|\psi\rangle}. \tag{18}$$

The binding energy E_b is given as:

$$E_b = E_e^{1s} - E_{D^0}. \tag{19}$$

Generally, the photoionization cross section (PCS) in low-dimensional system describes the transitions between the impurity ground state as an initial state and the subband as final state. Its formula, in the standard dipolar approximation, writes: [64,65]:

$$\sigma(\hbar\omega) = \frac{4\pi^2}{n_r}\alpha_{FS}\left(\frac{F_{\text{eff}}}{F_0}\right)^2\left(\frac{m_e^*}{m_0^*}\right)^2\hbar\omega\sum|\langle\psi_i|\overline{\zeta}-r^-|\psi_f\rangle|^2 \times\delta\left(E_f-E_i-\hbar\omega\right) \tag{20}$$

n_r is the refractive index material, $\alpha_{FS}=e^2/\hbar c$ is the fine structure constant [66] and $\hbar\omega$ is the photon energy. F_{eff}/F_0 is the effective field ratio; F_{eff} is the effective dielectric field of a transition while F_0 is the average field in the medium [67]. $\langle\psi_i|\overline{\zeta}\,\overline{r_e}|\psi_f\rangle$ is the dipole moment matrix element of the concerned states, where ζ is polarization vector of light wave. ψ_i is the initial state wavefunction given by equation (19) and ψ_f is the final state given by equations (12) and (13).

In collisional mode which corresponds to our case, the delta δ, in equation (20), can be replaced by the Lorentzian function as follow [68,69]:

$$\delta\left(E_f-E_i-\hbar\omega\right)\rightarrow\frac{I_{fi}\Gamma}{\left(E_b-\hbar\omega\right)^2+\Gamma^2} \tag{21}$$

where Γ is the impurity line-width and I_{fi} is the optical integral whites as:

$$I_{if} = \left|\int_v \psi_{D^0}(r,\theta,\phi)\psi_e(r)r\cos\theta d\tau\right|^2. \tag{22}$$

To calculate the PCS, we need to calculate the effective field parameter F_{eff}, which is not evident due to the inhomogeneity of impurity site and to its three spatial components for each direction of polarization of external radiation. To obtain a local field dependence in 3D spatial a self-consistent calculations are done [70,71]. The effective field ratio ($\frac{F_{\text{eff}}}{F_0}$), which can be obtained by adjusting the theoretical curve with experimental one, may be small or big depending on the electrons bound energy if it's weak or strong respectively. As far as we know, there are no experimental results for the impurity PCS in CSQD structure to doing comparison, and based on the fact that the cross section shape is not affected by the effective field ratio, thus, we take $\frac{F_{\text{eff}}}{F_0}=1$ [72,73]. Thereby, the final PCS expression writes:

$$\sigma(\hbar\omega)=\frac{4\pi^2\alpha_{FS}}{n_r}\left(\frac{m_e^*}{m_0^*}\right)^2\frac{\hbar\omega\Gamma\left|\int_v\psi_{D^0}(r,\theta,\phi)\psi_e(r)r\cos\theta d\tau\right|^2}{\left(E_b-\hbar\omega\right)^2+\Gamma^2}. \tag{23}$$

3 Results and discussions

As mentioned above, the aim of this work is analyzing the impact of non-parabolicity band, the electron-LO-phonon interaction, in-shell impurity position and the dielectric mismatch perturbations on the PCS of an ionized donor in *GaN*/*InN* CSQD. Table 1 presents the input parameters of materials involved in the calculation.

As we study the effects of the LO-phonon, *DMM* and the conduction band form (*PB* or *NPB*), it is important to us to understand how these contributions behave. Figure 2 shows the variation of phonons and *DMM* energies as function of the core radius (a) for $b=2a_D$ with and without the NPB model. DMM energy is calculated for two different external medium materials: SiO_2 ($\varepsilon_{\text{out}}=3.9$) and $BiTO_3$ ($\varepsilon_{\text{out}}=3.9$).

Seeing curves, it can be readily remarked that both terms, whatever the core radius value, have a negative contribution. Starting by phonon energy (Fig. 2a), we can remark that this term decreases as the core radius increases which means, in absolute value, that the interaction is more important in the strong confinement case. Regarding the *NPB* case, it conserves the same tendency but with an important increase, in absolute value, compared to the *PB* case. This is due to the fact that the *NPB* induces a strong correlation between the donor and LO-phonons. Also, we can notice that the gap between *PB* and *NPB* curves increases as the core radius increases, in other words it increases when the confinement get stronger.

For the aim to approaching the real situation, we have introduced the *DMM* effect in our approach. This contribution is summarized in Figure 2b. The variation of *DMM* is given for $b=2a_D$ and for both cases, with and without the parabolic band hypothesis. From this figure,

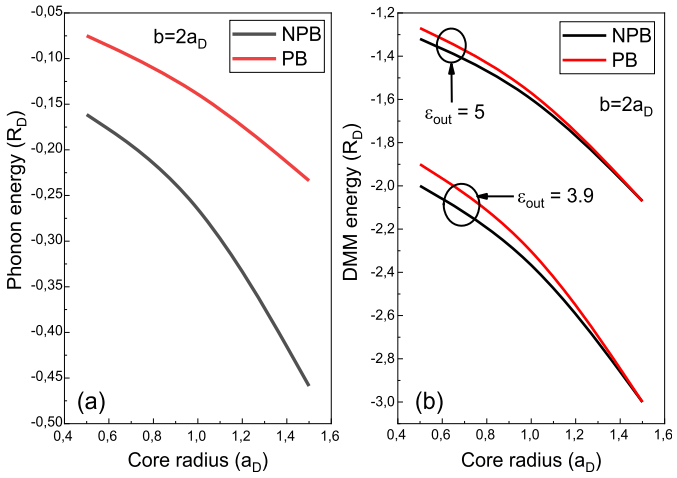

Fig. 2. Variation of phonons (a) and DMM (b) energies versus the core radius for $b = 2aD$ with and without NPB effect.

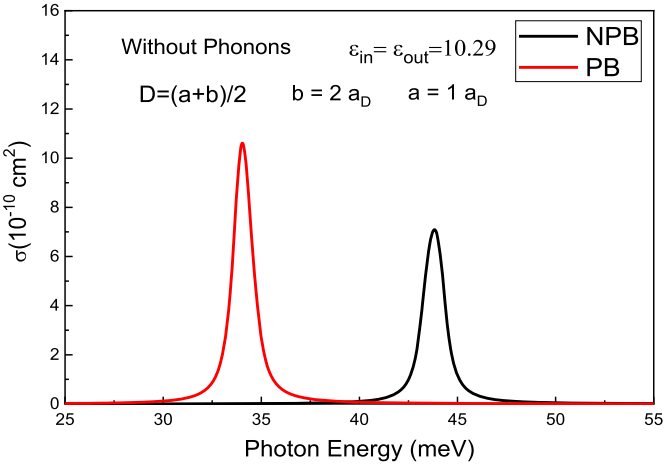

Fig. 4. Photoionization cross section as a function of the incident photon energy for $a = 1aD$, $b = 2aD$ with and without parabolicity band effect.

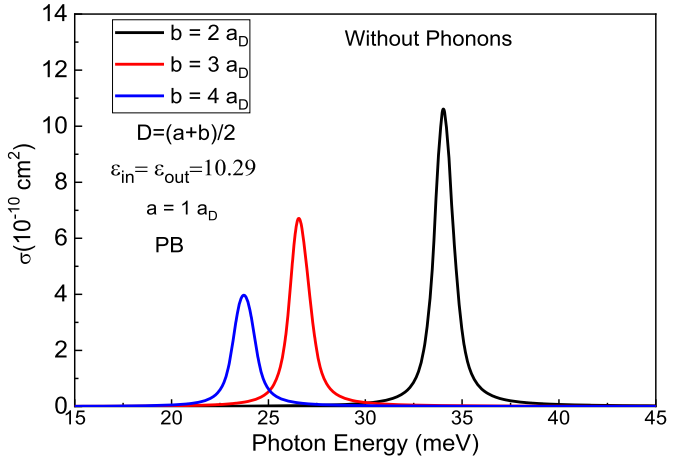

Fig. 3. Photoionization cross section as a function of the incident photon energy for different values of the outer radius b.

we can note that the effects of the polarization charges has an attractive character, it has negative values whatever the confinement strength (the core radius value). It depends on the well size; in absolute value, it is more important in the strong confinement case. Besides, the comparison between *PB* and *NPB* curves shows a confinement dependent. For the weak confinement the *NPB* effect on *DMM* is more important, as the core radius increases as it decreases and vanishes for $b - a = 0.5a_D$. It should be noted that the *NPB* influence is more remarkable when the difference between the dielectric constant of the structure and that of the external medium is too important.

Now, we will turn our attention to the *PCS* which is the main subject of this paper. To check the validity of our calculations we begin by analyzing the PCS without perturbations.

In the following, the use of red shift and blue shift means left and right displacement of the resonant peak respectively. Figure 3 presents the *PCS* versus the incident photon energy for fixed inner radius $a = 1a_D$ and different shell sizes $b = 2$, 3 and $4a_D$. As stated in equation (20), the PCS depends to the term $(\hbar\omega\Gamma)/((E_b - \hbar\omega) + \Gamma^2)$ and the peak of resonant corresponds to the condition $(E_b - \hbar\omega)^2 + \Gamma^2 = 0$. The curves show that the resonant peaks shift to the low photon energy values as the well width increases. This has a link with the weak geometric confinement obtained by increasing the shell dimension. The electron-donor binding and wave function tends to be expanded, which diminishes the binding energy and involves the peaks red shift. Moreover, decreasing the shell size, the peaks intensity increases. Indeed, the strong confinement pushes the wave function to be localized around the donor in the shell center which improves considerably the binding energy and then the matrix element.

Let's us add to our problem the *NPB* effect and see what happens. For that, we have plotted in Figure 4 the *PCS* as function of incoming photon energy with and without the *NPB* effect for $a = 1a_D$ and $b = 2a_D$. Observing the curves we can notice that the influence of *NPB* has blue shifted the peaks which is match perfectly with what we found and discussed in the first part. Indeed, the introduction of *NPB* enhances the binding energy [38], thus moves the threshold energy to the right side. Regarding the peaks intensity, it's clear that *NPB* diminishes it. This can be attributed to shrink the wave function which weakens the optical integral.

To investigate the simultaneous *NPB* and polaronic effects in *PCS*, we have kept the first and introduced the second. Figure 5 shows the variation of *PCS* as function of incident photon energy with and without phonon effect for $a = 1a_D$, $b = 2a_D$ and $D = (a + b)/2$ and for both *PB* (a) and *NPB* (b). It's clearly apparent, for all shell sizes, that the resonant peaks are red shifted under the phonon effect. Actually, this is expected remembering, based on our previous works [38], that the renormalized phonon energy contribution (Eq. (9)) causes a decrease in system total energy.

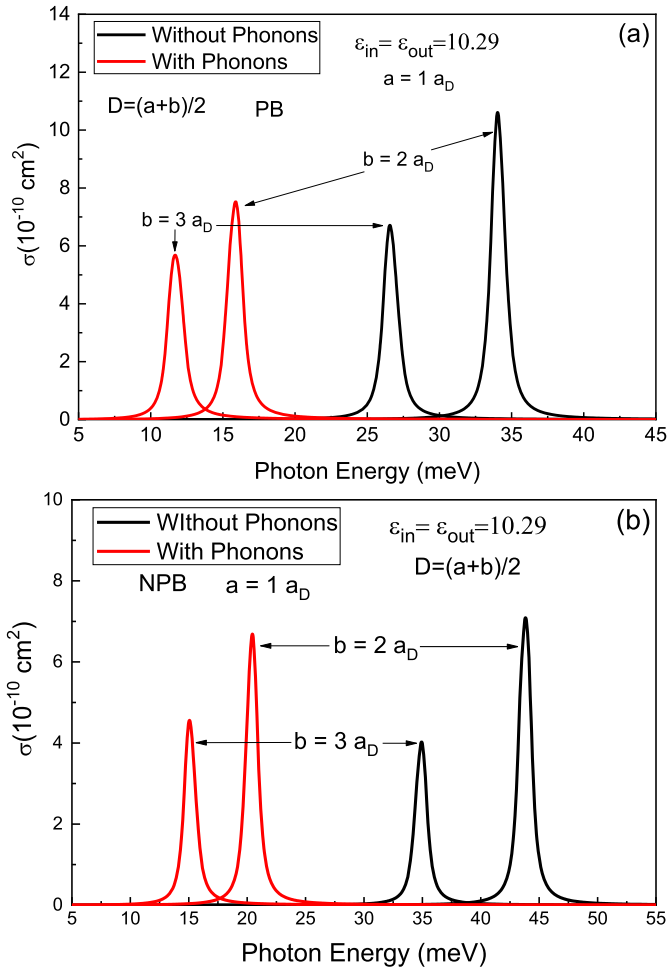

Fig. 5. Photoionization cross section as a function of the incident photon energy with and without polaronic corrections for two different values of the outer radius b: with (a) and without (b) parablicity band effect.

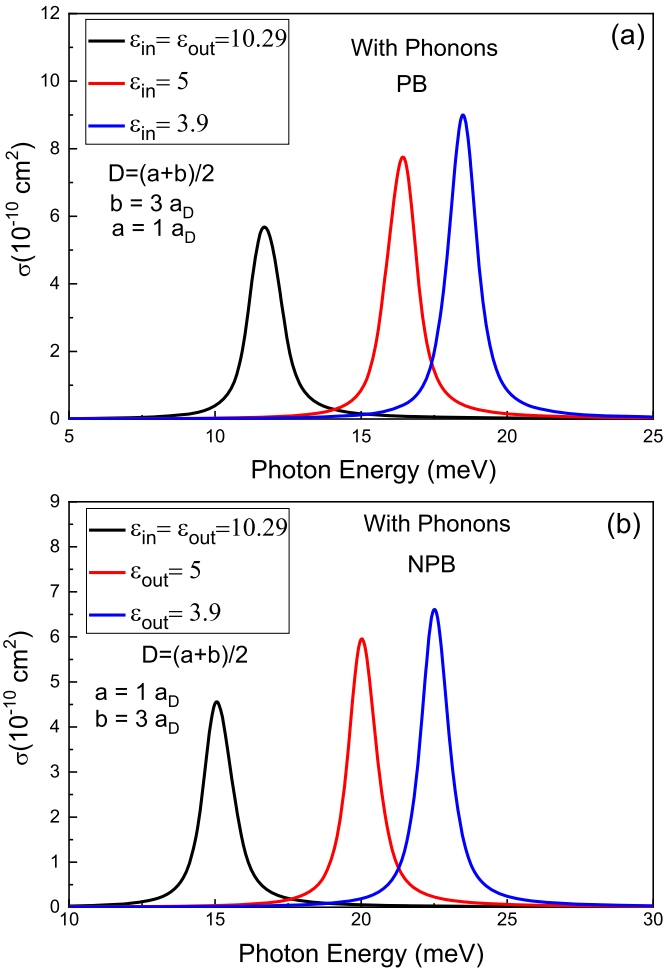

Fig. 6. Photoionization cross section versus the incoming photon energy for different values of dielectric constant including phonon contribution for $a = 1$ and $b = 3$ with and without parabolic band model.

This explains the spectrum red shift. We point out that the displacement of resonant peaks is more pronounced in *NPB* case than *PB* one. This is due to the opposite effect of *NPB* and phonon, the first causes a blue shift whereas the second a red shift, so their combination implies more peaks displacement. In addition, the electron-phonon interaction keeps the decreasing behavior of the peaks amplitude but lower than *NPB* did. May we search for the reason in the renormalized carrier mass (Eq. (1)) which is bigger than the conduction *NPB* effective one. This may explain the intensity diminishing.

Taking another step ahead, we have add to the two first effects the contribution of dielectric mismatch by considering three different values of external medium dielectric constant $\varepsilon_{out} = 3.9$, $\varepsilon_{out} = 5$ and $\varepsilon_{in} = \varepsilon_{out} = 10.29$.

Figure 6 shows the *PCS* versus photon energy taking into account the electron-donor-phonon coupling with and without the *NPB* effect for $a = 1a_D$, $b = 2a_D$ and for different values of dielectric constant mentioned above. It is readily apparent that for both cases (a) and (b) the *DM* influence shifts the threshold energy to the high values of photon energy even in the presence of polaronic interactions. Keeping in mind that, according to equation (4), the *DM* effect plays the role of a negative energy that attracts more the electron to the donor center, we can notice that there is a competition between phonons and *DM* effects. Seeing the curves we can say that the *DM* one has winning, especially in Figure 6b in which it benefited from *NPB* support. Another point to underline is that as under the others effects the peaks intensity decreases when introducing the external environment influence. This can be explained by the fact that the strong electron-donor coupling resulting from the dielectric contrast diminishes $e - D$ distance which affects the wave function and I_{fi}, thus makes peaks intensity falling.

Another effect that worth to be discussed is that of the donor position. For that we have chosen, beside the shell-center position, two significant positions, $D = a$ and $D = b$ which correspond to the core and shell edges respectively.

Figure 7 exhibits the *PCS* variation as function of incident photon energy keeping phonon, *NPB* and dielectric contrast effects. For $a = 1a_D$, $b = 2a_D$ and for different impurity positions. Observing the curves we can

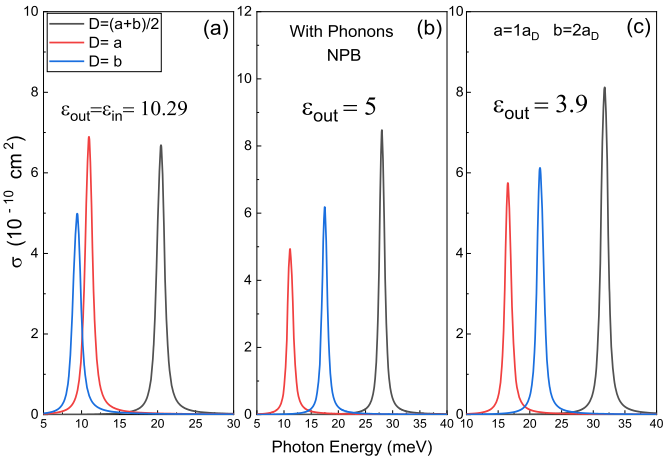

Fig. 7. Photoionization cross section as a function of the incident photon energy for different donor positions taking into account phonons and NPB effects.

remark that the on-center-shell impurity position $(D=(a+b)/2)$ pushes considerably the threshold energy of the *PCS* to higher energies. This is due to the high electron-donor coupling in this position compared to the others positions$(D=a \ \ or \ \ D=b)$.

Furthermore, we have noticed that without the *DM* effect (Fig. 6a) the peaks intensity has grown for $D=b$ case. So, although there is a redshift, the important increasing character of I_{fi} had the control over the peaks intensity. On the other side, introducing the external medium perturbation, the *PCS* keeps the same tendency of peaks displacement but not for peaks intensity which had a decrease behavior caused by the dielectric contrast. Actually, this is match well with results founding above.

4 Conclusion

In this work we have tried to do a complete investigation concerning the photoionization cross section on a single donor impurity in *GaN*/*InN* core/shell type-I inversed quantum dot taking into consideration all internal perturbation: the conduction band non-parabolicity, polaronic corrections, dielectric mismatch and donor position. All calculations are done in the framework of effective-mass and non-parabolic approximations. We have used a variational approach and assumed a finite potential confinement. The analysis of obtained curves reveals interesting results. Decreasing the well width, which means decreasing the confinement strength, shifts the *PCS* resonant peaks to the low energies and increases their peaks intensity. The phonon effect red shifts the *PCS* spectra while the influence of *NPB* blue shifts them which reflects the competition between them. Concerning the peaks intensity, the two effects make them fall *NPB* one did it more due to its large renormalized carrier mass. The *DM*effect acts as the *NPB* did and blue shifts the threshold energy even in polaronic interactions presence. According to different impurity position results and neglecting the *DM* effect we can notice that the $D=(a+b)/2$ position shifts the peaks to high energy and $D=b$ position increases their intensity. We hope that all these conclusions help to more understanding this effects on core/shell structures.

The authors wish to thank:
– The project of Hassan II Academy of Science and Technology project.
– Moroccan Ministry of Higher Education end Research and CNRST in the framework of PPR/37/2015 project.

Author contribution statement

– Conceptualization: Abdelali Talbi, Mohamed El Haouari, El Mustapha Feddi
– Formal analysis: Abdelali Talbi, Mohamed El Haouari
– Funding acquisition: Khalid Nouneh, Mohammed Addou, El Mustapha Feddi
– Investigation: Abdelali Talbi, Mohamed El Haouari
– Methodology: Mohamed El Haouari, Abdelali Talbi
– Project administration: El Mustapha Feddi, Khalid Nouneh, Mohammed Addou
– Resources: Abdelali Talbi, Mohamed El Haouari
– Validation: El Mustapha Feddi, Khalid Nouneh, Mohammed Addou
– Writing – original draft: Abdelali Talbi, Mohamed El Haouari
– Writing – review & editing: Khalid Nouneh, El Mustapha Feddi, Mohammed Addou

References

1. A.I. Ekimov, Al.L. Efros, A.A. Onushchenko, Solid State Commun. **56**, 921 (1985)
2. D. Vasudevan, R. Ranganathan, A. Trinchi, I. Cole, J. Alloys Compd. **636**, 395 (2015)
3. J.Q. Grim, L. Manna, I. Moreels, Chem. Soc. Rev. **44**, 5897 (2015)
4. H. Zhao, L. Jin, Y. Zhou, A. Bandar, Z. Fan, A.O. Govorov, Z. Mi, S. Sun, F. Rosei, A. Vomiero, Nanotechnology **27**, 495405 (2016)
5. W. Ji, P. Jing, W. Xu, X. Yuan, Y. Wang, J. Zhao, A. K.-Y. Jen, Appl. Phys. Lett. **103**, 053106 (2013)
6. T.-R. Kuo, S.-T. Hung, Y.-T. Lin, T.-L. Chou, M.-C. Kuo, Y.-P. Kuo, C.-C. Chen, Nanoscale Res. Lett. **12**, 537 (2017)
7. M. Marceddu, M. Saba, F. Quochi, A. Lai, J. Huang, D.V. Talapin, A. Mura, G. Bongiovanni, Nanotechnology **23**, 15201 (2012)
8. S. Rawalekar, M.V. Nikhil Raj, H.N. Ghosh, Sci. Adv. Mater. **4**, 637 (2012)
9. Z. Pan, H. Zhang, K. Cheng, Y. Hou, J. Hua, X. Zhong, ACS Nano, **6**, 3982 (2012)
10. L.P. Balet, S.A. Ivanov, A. Piryatinski, M. Achermann, V.I. Klimov, Nano Lett. **4**, 1485 (2004)
11. S.A. Ivanov, A. Piryatinski, J. Nanda, S. Tretiak, K.R. Zavadil, W.O. Wallace, D. Werder, V.I. Klimov, J. Am. Chem. Soc. **129**, 11708 (2007)
12. M. Schmidt, M. Grün, S. Petillon, E. Kurtz, C. Klingshirn, Appl. Phys. Lett. **77**, 85 (2000)

13. B. Mahler, P. Spinicelli, S. Buil, X. Quelin, J.-P. Hermier, B. Dubertret, Nature Mater. **7**, 659 (2008)
14. O. Chen, J. Zhao, V.P. Chauhan, J. Cui, C. Wong, D.K. Harris, H. Wei, H.-S. Han, D. Fukumura, R.K. Jain, M.G. Bawendi, Nature Mater. **12**, 445 (2013)
15. D. Canneson, L. Biadala, S. Buil, X. Quélin, C. Javaux, B. Dubertret, J.P. Hermier, Phys. Rev. B **89**, 035303 (2014)
16. C.M. Tyrakowski, A. Shamirian, C.E. Rowland, H. Shen, A. Das, R.D. Schaller, P.T. Snee, Chem. Mater. **27**, 7276 (2015)
17. X. Jin, J. Bai, X. Gu, C. Chang, H. Shen, Q. Zhang, F. Li, Z. Chen, Q. Li, Opt. Mater. Express **7**, 4395 (2017)
18. D. Dorfs, S.G. Hickey, A. Eychmüller, in *Type-I and Type-II core-shell quantum dots: synthesis and characterization, in Semiconductor Nanomaterials*, edited by C.S.S.R. Kumar (Wiley-VCH, Weinheim, 2010, pp. 331–366)
19. H. El Ghazi, A. Jorio, I. Zorkani, Physica B Condens. Matt, **427**, 106 (2013)
20. P. Ganesan, L. Senthilkumar, Physica E **74**, 204 (2015)
21. A. Elkadadra, D. Abouelaoualim, A. Oueraigli, A. Outzourhit, Optoelectron. Adv. Mater. **8**, 374 (2014)
22. W.-H. Liu, Y. Qu, S. L. Ban, Superlattices Microstruct. **102**, 373 (2017)
23. N.E. Christensen, I. Gorczyca, Phys. Rev. B **50**, 7 (1994)
24. Y.K. Kuo, J.Y. Chang, M.C. Tsai, S.H. Yen, Appl. Phys. Lett. **95**, 011116 (2009)
25. T. Shinada, S. Okamoto, T. Kobayashi, I. Ohdomari, Nature **437**, 1128 (2005)
26. P.M. Koenraad, M.E. Flatté, Nature Mater. **10**, 91 (2011)
27. D. Mocatta, G. Cohen, J. Schattner, O. Millo, E. Rabani, U. Banin, Science **332**, 77 (2011)
28. F. Dujardin, E. Feddi, E. Assaid, A. Oukerroum, Eur. Phys. J. B **74**, 507 (2010)
29. V.A. Fonoberov, A.A. Balandin, Appl. Phys. Lett. **85**, 5971 (2004)
30. V.A. Fonoberov, A.A. Balandin, Phys. Rev. B **70**, 195410 (2004)
31. L. Dallali, S. Jaziri, J. Martinez-Pastor, Solid State Commun. **209–210**, 33 (2015)
32. M.A. Stroscio, M. Dutta, *Phonons* in Nanostructures (Cambridge University Press, Cambridge, 2003)
33. C. Trallero-Giner, R. Pérez-Álvarez, F. García-Moliner, *Long Wave Polar Modes in Semiconductor Heterostructures* (Elsevier, Oxford, 1998)
34. B.K. Ridley, in *Electrons and Phonons in Semiconductor Multilayers*, 2nd edn. (Cambridge University Press, Cambridge, 2009)
35. E. Feddi, M. El Haouari, E. Assaid, B. Stébé, J. El Khamkhami, F. Dujardin, Phys. Rev. B **68**, 235313 (2003)
36. E. Feddi, M. El Haouari, E. Assaid, B. Stébé, J. El Khamkhami, F. Dujardin, Phys. Status Solidi B **240**, 106 (2003)
37. A. Sali, J. Kharbach, A. Rezzouk, M. Ouazzani Jamil, Superlattices Microstruct. **104**, 93 (2017)
38. M. El Haouari, M.E. Mora-Ramos, A. Talbi, E. Feddi, F. Dujardin, Physica E **103**, 188 (2018)
39. P.G. Bolcatto, C.R. Proetto, Phys. Rev. B **59**, 12487 (1999)
40. V.I. Boichuk, I.V. Bilynsky, I.O. Shakleina, I.P. Kogoutiouk, J. Phys. Conf. Ser. **289**, 012004c (2011)
41. A.L. Vartanian, A.L. Asatryan, L.A. Vardanyan, Superlattices Microstruct. **103**, 205 (2017)
42. N. Sil, N. Daripa, A. Kapoor, S.K. Dey, Pramana-J. Phys. **90**, 7 (2018)
43. M. Cristea, E.C. Niculescu, Eur. Phys. J. B **85**, 191 (2012)
44. E.C. Niculescu, M. Cristea, U.P.B. Sci. Bull. Series A **75**, 195 (2013)
45. E.C. Niculescu, M. Cristea, J. Lumin. **135**, 120 (2013)
46. M. Cristea, A. Radu, E.C. Niculescu, J. Lumin. **143**, 592 (2013)
47. A.L. Vartanian, A.L. Asatryan, L.A. Vardanyan, Superlattices Microstruct. **113**, 442 (2018)
48. S. M'zerd, A. Talbi, M. Bikerouin, M. El Haouari, N. Aghoutane, M. El-Yadri, E. Feddi, J. Mater. Res. **35**, 2077 (2020)
49. S. Hong, J. Singh, J. Appl. Phys. **61**, 5346 (1987)
50. C. Aldrich, K.K. Bajaj, Solid State Commun. **22**, 157 (1977)
51. J.T. Devreese, *Polarons in ionic crystals and polar semiconductors: Antwerp Advanced Study Institute 1971 on Fröhlich Polarons and Electron-phonon interaction in polar semiconductors* (North-Holland, Pub. Co., Amsterdam: 1972)
52. H. Fröhlich, Proc. R. Soc. Edinburgh, Sect. A Math. **215**, 291 (1952)
53. T.D. Lee, F.E. Low, D. Pines, Phys. Rev. **90**, 2 (1953)
54. S. Shokhovets, O. Ambacher, G. Gobsch, Phys. Rev. B **76**, 125203 (2007)
55. Gh. Safarpour, M.A. Izadi, M. Novzari, E. Niknam, M.M. Golshan, Commun. Theor. Phys. **61**, 765 (2014)
56. A. Radosavijevi¢, J. Radovanovi¢, V. Milanovi¢, D. Indjin. Opt. Quant. Electron. **47**, 865 (2015)
57. H. El Ghazi, A. John Peter, Physica B **470-471**, 64 (2015)
58. K. Albert Wang, C. Lian, N. Su, D. Jena, J. Timler, Appl. Phys. Lett. **91**, 232117 (2007)
59. M. K. Bose, K. Midya, C. Bose, J. Appl. Phys. **101**, 054315 (2007)
60. J. Pollmann, H. Bünttner, Phys. Rev. B **16**, 4480 (1977)
61. A.A. Parvathi, A. John Peter, Acta Phys. Pol. A **124**, 706 (2013)
62. A. Zouitine, A. Ibral, E. Assaid, F. Dujardin, E. Feddi, Superlattices Microstruct. **109**, 123 (2017)
63. A. Ibral, A. Zouitine, E. Assaid, E. Feddi, F. Dujardin, J. Optoelectron. Adv. Mater. **17**, 151 (2015)
64. M. Lax, Proceedings of the Atlantic City Conference on Photoconductivity (John Wiley Sons, New York, 1956)
65. M.G. Barseghyan, A. Hakimyfard, S.Y. López, C.A. Duque, A.A. Kirakosyan, Physica E **42**, 1618 (2010)
66. A. El Aouami, E. Feddi, A. Talbi, F. Dujardin, C.A. Duque, Appl. Phys. A, **124**, 124 (2018)
67. B.K. Ridley, Quantum Processes in Semiconductors (Clarendon Press, Oxford, 1982)
68. I.N. Bronshtein, K.A. Semendyayev, G. Musiol, H. Mühlig, Handbook of Mathematics (Springer-Verlag, Berlin Heidelberg, 2007)
69. J.-M. Malherbe, in Initiation à la Physique du Soleil, diagnostics spectroscopiques et polarimétriques, effets Doppler et Zeeman (Meudon, France, 2014, p. 70)
70. V. Lozovski, V. Piatnytsia, J. Comput. Theor. Nanosi. **8**, 1 (2011)

71. O. Keller, Phys. Rep. **268**, 85 (1996)
72. A. Sali, M. Fliyou, H. Loumrhari, J. Phys. Chem. Solids **59**, 625 (1998)
73. M. El-Said, M. Tomak, J. Phys. Chem. Solids **52**, 603 (1991)
74. P. Rinke, M. Winkelkemper, A. Qteish, D. Bimberg, J. Neugebauer, M. Scheffer, Phys. Rev. B **77**, 075202 (2008)
75. M. Feneberg, M. Röppischer, C. Cobet, N. Esser, J. Schörmann, T. Schupp, D.J. As, F. Hörich, J. Bläsing, A. Krost, R. Goldhahn, Phys. Rev. B **85**, 155207 (2012)
76. M.-Y. Xie, M. Schubert, J. Lu, P.O.Å. Persson, V. Stanishev, C.L. Hsiao, L.C. Chen, W. J. Schaff, V. Darakchieva, Phys. Rev. B **90**, 195306 (2014)
77. R. Cuscó, N. Domènecsh-Amador, S. Novikov, C.T. Foxom, L. Artús, Phys. Rev. B **92**, 075206 (2015)

Cite this article as: Abdelali Talbi, Mohamed El Haouari, Khalid Nouneh, El Mustapha Feddi, Mohammed Addou, Impact of conduction band non-parabolicity and dielectric mismatch on photoionization cross section of donor bound polaron in spherical GaN/InN core-shell nanoparticle, Eur. Phys. J. Appl. Phys. **93**, 10401 (2021)